The Journal of Chemical Physics

The effect of ion pairs on coacervate-driven self-assembly of block polyelectrolytes

Cite as: J. Chem. Phys. **154**, 144903 (2021); https://doi.org/10.1063/5.0044845
Submitted: 20 January 2021 • Accepted: 30 March 2021 • Published Online: 13 April 2021

Jiadi Jiang, Er-Qiang Chen and Shuang Yang

The Journal of Chemical Physics ARTICLE scitation.org/journal/jcp

The effect of ion pairs on coacervate-driven self-assembly of block polyelectrolytes

Cite as: J. Chem. Phys. 154, 144903 (2021); doi: 10.1063/5.0044845
Submitted: 20 January 2021 • Accepted: 30 March 2021 •
Published Online: 13 April 2021

Jiadi Jiang, Er-Qiang Chen,[a] and Shuang Yang[b]

AFFILIATIONS

Beijing National Laboratory for Molecular Sciences, Department of Polymer Science and Engineering and Key Laboratory of Polymer Chemistry and Physics of Ministry of Education, College of Chemistry, Peking University, Beijing 100871, People's Republic of China

[a]Electronic mail: eqchen@pku.edu.cn
[b]Author to whom correspondence should be addressed: shuangyang@pku.edu.cn

ABSTRACT

The incorporation of oppositely charged polyelectrolytes into a block copolymer system can lead to formation of microphase separated nanostructures driven by the electrostatic complex between two oppositely charged blocks. It is a theoretical challenge to build an appropriate model to handle such coacervate-driven self-assembly, which should capture the strong electrostatic correlations for highly charged polymers. In this paper, we develop the self-consistent field theory considering the ion paring effect to predict the phase behavior of block polyelectrolytes. In our model, two types of ion pairs, the binding between two oppositely charged monomers and the binding between charged monomers and counterions, are included. Their strength of formation is controlled by two parameters K_{aa} and K_{ac}, respectively. We give a detailed analysis about how the binding strength K_{ac} and K_{aa} and salt concentration affect the self-assembled nanostructure of diblock polyelectrolyte systems. The results show that the binding between two oppositely charged blocks provides driven force for microphase separation, while the binding between charged monomers and counterions competes with the polyion pairing and thus suppresses the microphase separation. The addition of salt has a shielding effect on the charges of polymers, which is a disadvantage to microphase separation. The phase diagrams as a function of polymer concentration and salt concentration at different situations are constructed, and the influence of K_{aa}, K_{ac}, and charged block composition f_a is analyzed in depth. The obtained phase diagrams are in good agreement with currently existing experimental and theoretical results.

I. INTRODUCTION

Polyelectrolyte complexation is a liquid–liquid phase-separated phenomenon occurred in the system consisted of two oppositely charged polyelectrolyte.[1–13] When two oppositely charged polyelectrolytes are blended in aqueous solution, the system will undergo macroscopic phase separation into a polymer-dense "coacervate" phase and a polymer-dilute "supernatant" phase[8] driven by the electrostatic interaction between two oppositely charged chains and the entropy gains from the release of counterions associated with the chains.[9,10] When such oppositely charged polyelectrolytes are conjugated with a neutral polymer block, microphase separation may happen and a variety of nanostructures, including micelles and long-range ordered phases, may be formed.[14–25] The liquid coacervation materials may behave like "transient hydrogels" that are essentially cross-linked by electrostatic interaction.[26,27] These self-assembled structures are sensitive to many controlling factors (salt concentration, pH, temperature, linear charge density or charge sequence of polymers, and polymer concentration), which allows for facile tuning the material properties and leads to wide biomaterial applications varying from bioadhesives,[28] tissue growth scaffolds,[29–31] and modeling of membraneless organelles[32] to drug delivery.[33–36]

A number of experimental studies have handled the self-assembled morphologies driven by complex coacervate motifs. At low polymer concentrations, diblock or triblock copolyelectrolytes can form disordered spherical micelles as expected.[37,38] Further increasing the polymer concentrations results in a variety of long-range ordered structures of the polyelectrolyte complex from

body-center cubic spheres to hexagonally close-packed cylinders to lamellae, and a few of phase diagrams in salt vs polymer concentration space were obtained.[27,39–43] For neutral block copolymers, the microphase separation is due to the immiscibility between different blocks (generally represented by a large χ parameter). However, the distinct effect of increasing polymer concentration on the scattering pattern evolution reveals that coacervate-driven assembly obeys a significantly different mechanism from the well understood assembly of neutral block copolymers.[27] The salt typically screens the electrostatic interactions, which plays an important role in determining the phase behavior of coacervate-driven assembly.

Due to the electrostatic correlation nature of complex coacervation, it is difficult to deal with such coacervate-driven self-assembly theoretically. Now, it has been recognized that the driven force for complex coacervation of oppositely charged polymers comes from the Debye–Huckel-like attraction induced by electrostatic fluctuation for the system with low linear charge density, [44,45] whereas it mainly results from the entropy gained by release of counterions for highly charged polymers.[46,47] Most theoretical studies focus on the macrophase separation phenomena[9,48–56] or microphase separated ordered phases[57] of homopolyelectrolyte coacervation. On the other hand, a little theoretical work has been done toward on coacervate-driven self-assembly of block copolyelectrolytes.[42,58–62] Different from the χ-driven microphase separation of the neutral system, coacervate-driven self-assembly mainly arises from the electrostatic correlations between charged blocks. For symmetric charged block copolymers, the electrostatic complexation between oppositely charged blocks leads to the uniform spatial distributions of total charges and electrostatic potential. In this case, the usual self-consistent field theory (SCFT) fails to describe correctly the microphase separated structure as the result of mean field treatment to electrostatic interactions (zero electrostatic energy due to complete compensation of positive and negative charges). The electrostatic correlations need to be taken into account. Rumyantsev *et al.* used a scaling theory to consider the coacervate-driven micellization at low polymer concentration and low linear charge density limit.[63] The first theoretical study for ordered morphologies is given by Audus *et al.*[42] They developed a modified SCFT with an embedded fluctuation (EF) model in which the one-loop random phase approximation (RPA) is used in order to capture the electrostatic correlations. Using this EF model, they investigated the phase diagrams of salt-free triblock copolyeletrolyte solutions as a function of end-block fraction and polymer concentration. The calculations using the EF model were consistent with small angle x-ray scattering (SAXS) measurements on an experimental system. In spite of the great success on understanding the hydrogel with an ordered structure, such an EF model containing Gaussian fluctuation contributions breaks down when the line charge density is relatively high, which limits its application.

Significant progress for coacervate self-assembly with high charge density polymers was achieved by Sing's group. They proposed a hybrid "Monte Carlo-single chain in mean field" (MC-SCMF) method to handle charge-dense scenarios.[58] Then, they embedded molecular-level Monte Carlo (MC) simulations into field theoretic calculations, leading to a multiscale, coarse-grained description to such systems. Their calculations match well with previous experimental and theoretical results. Recently, Ong and Sing developed a transfer matrix (TM) theory, and incorporated it into a SCFT calculation to provide predictions for both the macroscopic phase behavior and microscopic charge correlations present in complex coacervates.[60] The transfer matrix theory is based on a one-dimensional adsorption model and accounts for charge correlations related to ion pairing, counterion condensation, and release.[59] Their phase diagram predictions for the two dimensional system are analogous to experimental results in the literature.[41,64] This theory is easy to calculate and shows its novelty. However, their transfer matrix method involves a phenomenological parameter to describe the three-order term that captures excluded volume interaction between polymer species and salt ions in the coacervate phase, and it also neglects the spatial dependence of the transfer matrix of each segment along the chain in practical calculation.[60] In addition, a more accurate handling to the transfer matrix needs the help of simulations.[62]

In this paper, we develop a new method to predict the phase behavior of coacervate-driven self-assembly in the block polyelectrolyte system. Since there is ion pairing formation in a strong electrostatic correlation system, [55,65] we embed the formation of ion pairs into the SCFT model. Two types of ion pairs in such a coacervate-driven polyelectrolyte system are considered. One is the binding between two oppositely charged monomers on polymers, whose binding strength is represented by K_{aa}. Another one is the binding between charges on polymers and the corresponding counterions, whose binding strength is represented by K_{ac}. There exists a competition between two binding modes, which also depends on the salt concentration and polymer concentration. By the use of these two parameters K_{aa} and K_{ac}, we capture the essential physical features of electrostatic complexation between oppositely charged polyelectrolytes with high charge density. Consequently, we are capable of describing coacervate-driven self-assembly appropriately. Some interesting physical behaviors and insights are revealed.

We apply the method to calculate the ordered phases of coacervate-driven self-assembly of diblock polyelectrolytes. First, we will show the role of the binding strength K_{aa} and K_{ac} in self-assembled structures. The detailed spatial distribution of all species, including the ion pairs, can be obtained. The ordered microphases can be formed under the strong association between oppositely charged blocks, even for the low χ system. Second, we verify the screening effect of salt. Adding salts decreases the stability of ordered phases. Finally, we construct the phase diagrams as a function of polymer concentration and salt concentration at different K_{aa}, K_{ac}, and charged block fractions f_a. In particular, we find that salt concentration and K_{ac} are not independent parameters, and their product constitutes one controlling parameter in determining the phase diagram. We emphasis that our results are well comparable to the existing experimental and theoretical results, demonstrating that our method provides a good description for coacervate-driven self-assembly of charged polymers.

II. THEORETICAL MODEL

Consider a system consisting of two oppositely charged diblock copolyelectrolytes, water, and salt (see Fig. 1). The two copolyelectrolytes are assumed to be identical except for the sign of the charge. They are all modeled as continuous Gaussian chains and composed of two bead species (we denote by the labels A and B). Thus, we use A_1B_1 and A_2B_2 to represent two copolyelectrolytes, respectively. B_1

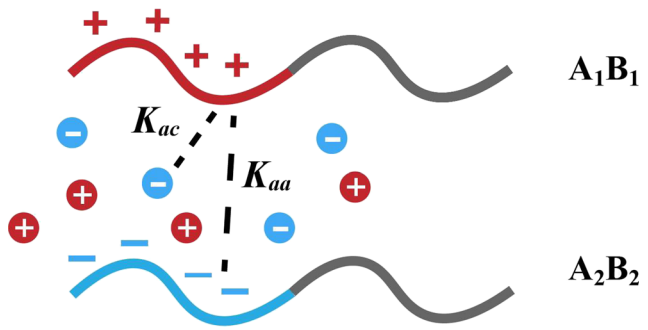

FIG. 1. Schematic diagram for formation of ion pairs in oppositely charged diblock polyelectrolytes. Due to the coacervate-driven attraction between two oppositely charged blocks, the copolyelectrolyte system can self-assemble into ordered structures through microphase separation between charged blocks and neutral blocks. The ion pairs can be formed between charged monomers and counterions or between oppositely charged monomers belonging different chains.

and B_2 blocks are neutral. For the A_1B_1 chain, the A block is positively charged, and the counterions (denoted as C_1) dissociated from it are anions. For the A_2B_2 chain, the A_2 block is negatively charged, and the dissociated counterions (denoted as C_2) are cations. For simplicity, the added salt ions here are assumed to be indistinguishable from counterions C_1 and C_2. In the following, we will express C_1 and C_2 as small ions. The water molecule is denoted by S.

The system volume is V. The chain numbers of A_1B_1 and A_2B_2 are n_{p1} and n_{p2}, respectively. The total degrees of polymerization for two copolymers are denoted by N_1 and N_2, respectively. In addition, the degrees of polymerization for A_1, B_1, A_2, and B_2 are denoted by N_{A_1}, N_{B_1}, N_{A_2}, and N_{B_2}, satisfying $N_{A_1} + N_{B_1} = N_1$ and $N_{A_2} + N_{B_2} = N_2$. Each monomer in A_1 and A_2 chains carries z_{A_1} and z_{A_2} elementary charges. Similarly, the valences of small ions C_1 and C_2 are z_{C_1} and z_{C_2}. The total numbers of C_1 and C_2 are denoted by n_{C_1} and n_{C_2}. The volumes of monomers A_1, B_1, A_2, and B_2, small ions C_1 and C_2, and water are denoted by v_{A_1}, v_{B_1}, v_{A_2}, v_{B_2}, v_{C_1}, v_{C_2}, and v_S, respectively. We assume $v_{A_1} = v_{A_2} = v_A$ and $v_{B_1} = v_{B_2} = v_B$. b_A and b_B are used to represent the Kuhn lengths of A and B monomers. In addition, we assume $b_A = b_B = b$ for simplicity. Therefore, the copolymer compositions (the volume fraction of the A block) for two copolymers are then given by $f_{A_1} = N_{A_1}v_A/(N_{A_1}v_A + N_{B_1}v_B)$ and $f_{A_2} = N_{A_2}v_A/(N_{A_2}v_A + N_{B_2}v_B)$, respectively.

The microscopic concentrations of A_1, B_1, A_2, B_2, C_1, C_2, and S in position $\mathbf{r}$ are given by

$$\hat{\rho}_\alpha(\mathbf{r}) = \sum_{i=1}^{n_p} \int_0^{N_\alpha} \mathrm{d}s\delta(\mathbf{r} - \mathbf{R}_i^\alpha(s)), \tag{1}$$

$$\hat{\rho}_\beta(\mathbf{r}) = \sum_{i=1}^{n_\beta} \delta(\mathbf{r} - \mathbf{r}_i^\beta), \tag{2}$$

where α denotes monomer species A_1, B_1, A_2, and B_2 and β denotes small ions C_1 and C_2 or water S. $\mathbf{R}_i^\alpha(s)$ represents the position of the s-th monomer at the α-block of the i-th polymer chain. $\mathbf{r}_i^\beta$ denotes the position of the i-th small molecule β.

The formation of ion pairs is accounted for explicitly in our model, which means the dynamic association between positive charge and negative charge occurs. We take the following reversible dynamic equilibrium into consideration:

$$\mathrm{A_1}^+ + \mathrm{C_1}^- \rightleftharpoons [\mathrm{A_1C_1}],$$
$$\mathrm{A_2}^- + \mathrm{C_2}^+ \rightleftharpoons [\mathrm{A_2C_2}],$$
$$\mathrm{A_1}^+ + \mathrm{A_2}^- \rightleftharpoons [\mathrm{A_1A2}].$$

Here, $[A_1C_1]$, $[A_2C_2]$, and $[A_1A_2]$ are the resulted ion pairs with corresponding equilibrium constants $K_{a_1c_1}$, $K_{a_2c_2}$, and $K_{a_1a_2}$ for these associated ion pairs. Therefore, there exists three different reaction sites on a charged A block, as shown in Fig. 1. These are charged site (denoted by a_1), uncharged site paired with C_1 (denoted by a_1c_1), and uncharged site paired with monomers from A_2 (denoted by a_1a_2). A_2 chain has the similar case, and the three sites are denoted by a_2, a_2c_2, and a_1a_2, respectively. Consequently, there are total five reaction sites on the A block in our system, and we use n_{a_1}, n_{a_2}, $n_{a_1c_1}$, $n_{a_2c_2}$, and $n_{a_1a_2}$ to denote their numbers. Finally, fractions of different sites, which give the ratio of the number of some sites to the number of total monomers (A_1 or A_2) locally, are defined as

$$\hat{f}_1(\mathbf{r}) = \sum_{i=1}^{n_{a_1}} \delta(\mathbf{r} - \mathbf{r}_i^{a_1})/\hat{\rho}_{A_1}(\mathbf{r}), \tag{3}$$

$$\hat{f}_2(\mathbf{r}) = \sum_{i=1}^{n_{a_2}} \delta(\mathbf{r} - \mathbf{r}_i^{a_2})/\hat{\rho}_{A_2}(\mathbf{r}), \tag{4}$$

$$\hat{g}_1(\mathbf{r}) = \sum_{i=1}^{n_{a_1c_1}} \delta(\mathbf{r} - \mathbf{r}_i^{a_1c_1})/\hat{\rho}_{A_1}(\mathbf{r}), \tag{5}$$

$$\hat{g}_2(\mathbf{r}) = \sum_{i=1}^{n_{a_2c_2}} \delta(\mathbf{r} - \mathbf{r}_i^{a_2c_2})/\hat{\rho}_{A_2}(\mathbf{r}), \tag{6}$$

$$\hat{h}_1(\mathbf{r}) = \sum_{i=1}^{n_{a_1a_2}} \delta(\mathbf{r} - \mathbf{r}_i^{a_1a_2})/\hat{\rho}_{A_1}(\mathbf{r}), \tag{7}$$

$$\hat{h}_2(\mathbf{r}) = \sum_{i=1}^{n_{a_1a_2}} \delta(\mathbf{r} - \mathbf{r}_i^{a_1a_2})/\hat{\rho}_{A_2}(\mathbf{r}). \tag{8}$$

Here, f_1, g_1, and h_1 represent the fractions of different reaction sites on the charged A_1 block and should satisfy $\hat{f}_1(\mathbf{r}) + \hat{g}_1(\mathbf{r}) + \hat{h}_1(\mathbf{r}) = 1$. The same relation applies to the charged A_2 block as $\hat{f}_2(\mathbf{r}) + \hat{g}_2(\mathbf{r}) + \hat{h}_2(\mathbf{r}) = 1$.

In this study, we use the semi-grand canonical ensemble to deal with the system. That is to say, the number of copolymer chains is fixed, while the numbers of other small molecules, including small ions and water solvents, are variable. The chemical potentials of small molecules are fixed and dependent of the values of the reservoir. The Hamiltonian is the sum of four contributions, $H = H_{ela} + H_{int} + H_{ele} + H_{chem}$. The first term H_{ela} is the elastic energy due to the stretching of polymer chains, which can be written as

$$H_{ela} = \sum_{\alpha=A_1,B_1} \sum_{i=1}^{n_{p1}} \frac{3}{2b^2} \int_0^{N_\alpha} \mathrm{d}s \left(\frac{\mathrm{d}\mathbf{R}_i^\alpha(s)}{\mathrm{d}s} \right)^2 + \sum_{\alpha=A_2,B_2} \sum_{i=1}^{n_{p2}} \frac{3}{2b^2} \int_0^{N_\alpha} \mathrm{d}s \left(\frac{\mathrm{d}\mathbf{R}_i^\alpha(s)}{\mathrm{d}s} \right)^2. \tag{9}$$

H_{int} is the incompatible interaction energy between different components. We ignore the excluded volume interactions related to counterions. Considering the homology of the A_1B_1 chain and A_2B_2 chain, H_{int} only includes the interaction contributions among A monomers, B monomers, and water molecules. Its form is as follows:

$$H_{int} = \int \mathrm{d}\mathbf{r}[\chi_{AB}\nu_A\nu_B\hat{\rho}_A(\mathbf{r})\hat{\rho}_B(\mathbf{r}) + \chi_{SA}\nu_S\nu_A\hat{\rho}_S(\mathbf{r})\hat{\rho}_A(\mathbf{r}) + \chi_{SB}\nu_S\nu_B\hat{\rho}_S(\mathbf{r})\hat{\rho}_B(\mathbf{r})]. \tag{10}$$

These parameters of χ_{AB}, χ_{SA}, and χ_{SB} are the Flory–Huggins interaction parameters between the A block and the B block, the B block and water, the A block and water, respectively. Since A_1 and A_2 are identical (also B_1 and B_2 are identical except their oppositely carried charges), the concentration of A monomers is defined as $\hat{\rho}_A(\mathbf{r}) = \hat{\rho}_{A_1}(\mathbf{r}) + \hat{\rho}_{A_2}(\mathbf{r})$ and concentration of B monomers is defined as $\hat{\rho}_B(\mathbf{r}) = \hat{\rho}_{B_1}(\mathbf{r}) + \hat{\rho}_{B_2}(\mathbf{r})$.

The term H_{ele} is the electrostatic contribution and can be written as

$$H_{ele} = \int \mathrm{d}\mathbf{r}\left(\beta e\psi(\mathbf{r})\hat{\rho}_e(\mathbf{r}) - \frac{1}{2}\beta\varepsilon|\nabla\psi(\mathbf{r})|^2\right), \tag{11}$$

where β is equal to $1/k_BT$. e is the elementary charge, and $\psi(\mathbf{r})$ is the electrostatic potential. $\hat{\rho}_e(\mathbf{r})$ is the charge density at position $\mathbf{r}$ and can be represented as $\hat{\rho}_e(\mathbf{r}) = z_{A_1}\hat{f}_1(\mathbf{r})\hat{\rho}_{A_1}(\mathbf{r}) + z_{A_2}\hat{f}_2(\mathbf{r})\hat{\rho}_{A_2}(\mathbf{r}) + z_{C_1}\hat{\rho}_{C_1}(\mathbf{r}) + z_{C_2}\hat{\rho}_{C_2}(\mathbf{r})$. ε is the dielectric constant, which is assumed to be spatial invariant in our model.

The last term H_{chem} is the chemical contribution derived from the chemical potentials of each species and has the form

$$\hat{H}_{chem} = \beta\int \mathrm{d}\mathbf{r}\Big[\mu_{a_1}\hat{f}_1(\mathbf{r})\hat{\rho}_{A_1}(\mathbf{r}) + \mu_{a_1c_1}\hat{g}_1(\mathbf{r})\hat{\rho}_{A_1}(\mathbf{r}) + \mu_{a_2}\hat{f}_2(\mathbf{r})\hat{\rho}_{A_2}(\mathbf{r}) + \mu_{a_2c_2}\hat{g}_2(\mathbf{r})\hat{\rho}_{A_2}(\mathbf{r}) + \mu_{a_1a_2}\hat{h}_1(\mathbf{r})\hat{\rho}_{A_1}(\mathbf{r}) + \mu_{C_1}\hat{\rho}_{C_1}(\mathbf{r}) + \mu_{C_2}\hat{\rho}_{C_2}(\mathbf{r}) + \mu_S\hat{\rho}_S(\mathbf{r})\Big]. \tag{12}$$

Here, μ_{a_1}, μ_{a_2}, $\mu_{a_1c_1}$, $\mu_{a_2c_2}$, and $\mu_{a_1a_2}$ are the chemical potentials of the corresponding species. Note that $\hat{h}_1(\mathbf{r})\hat{\rho}_{A_1}(\mathbf{r})$ is the density of the species a_1a_2 and satisfies $\hat{h}_1(\mathbf{r})\hat{\rho}_{A_1}(\mathbf{r}) = \hat{h}_2(\mathbf{r})\hat{\rho}_{A_2}(\mathbf{r})$. The chemical contributions from species B_1 and B_2 blocks are neglected because they are constant in the system.

The partition function then can be written in terms of the functional integral over all chain conformations and positions of all small molecules,

$$\begin{aligned} Z = \zeta\frac{1}{n_{p_1}!n_{p_2}!}\prod_m\sum_{n_m=0}^{\infty}\frac{1}{n_m!}\int \mathrm{D}\{\mathbf{R}^1(s)\}\,\mathrm{D}\{\mathbf{R}^2(s)\}\,\mathrm{D}\{\mathbf{r}_m\}\,\mathrm{D}\{\psi\}\exp(-H)\prod_{i=1}^{n_{p_1}}\delta(\mathbf{R}_i^{A_1}(N_{A_1}) - \mathbf{R}_i^{B_1}(N_{B_1}))\prod_{i=1}^{n_{p_2}}\delta(\mathbf{R}_i^{A_2}(N_{A_2}) - \mathbf{R}_i^{B_2}(N_{B_2}))\\ \times\prod_{\mathbf{r}}\delta\left(\sum_j\hat{\rho}_j(\mathbf{r})\nu_j - 1\right)\prod_{\mathbf{r}}\delta(\hat{f}_1(\mathbf{r})\hat{\rho}_{A_1}(\mathbf{r}) + \hat{g}_1(\mathbf{r})\hat{\rho}_{A_1}(\mathbf{r}) + \hat{h}_1(\mathbf{r})\hat{\rho}_{A_1}(\mathbf{r}) - \hat{\rho}_{A_1}(\mathbf{r}))\prod_{\mathbf{r}}\delta(\hat{f}_2(\mathbf{r})\hat{\rho}_{A_2}(\mathbf{r}) + \hat{g}_2(\mathbf{r})\hat{\rho}_{A_2}(\mathbf{r}) + \hat{h}_2(\mathbf{r})\hat{\rho}_{A_2}(\mathbf{r}) - \hat{\rho}_{A_2}(\mathbf{r}))\\ \times\prod_{k=1}^{n_{a_1}}\sum_{i=1}^{n_{p_1}}\int_0^{N_{A_1}}ds\delta(\mathbf{r}_k^{a_1} - \mathbf{R}_i^{A_1}(s))\prod_{k=1}^{n_{a_1c_1}}\sum_{i=1}^{n_{p_1}}\int_0^{N_{A_1}}ds\delta(\mathbf{r}_k^{a_1c_1} - \mathbf{R}_i^{A_1}(s))\prod_{k=1}^{n_{a_1a_2}}\sum_{i=1}^{n_{p_1}}\int_0^{N_{A_1}}ds\delta(\mathbf{r}_k^{a_1a_2} - \mathbf{R}_i^{A_1}(s))\\ \times\prod_{k=1}^{n_{a_2}}\sum_{i=1}^{n_{p_2}}\int_0^{N_{A_2}}ds\delta(\mathbf{r}_k^{a_2} - \mathbf{R}_i^{A_2}(s))\prod_{k=1}^{n_{a_2c_2}}\sum_{i=1}^{n_{p_2}}\int_0^{N_{A_2}}ds\delta(\mathbf{r}_k^{a_2c_2} - \mathbf{R}_i^{A_2}(s))\prod_{k=1}^{n_{a_1a_2}}\sum_{i=1}^{n_{p_2}}\int_0^{N_{A_2}}ds\delta(\mathbf{r}_k^{a_1a_2} - \mathbf{R}_i^{A_2}(s)). \end{aligned} \tag{13}$$

Here, ζ is the contribution due to the kinetic energy and is a constant. Subscript m runs over all types of small molecules and different sites on A chains. Subscript j represents all species in the system. The first two delta functions ensure the chain connectivity between A and B blocks. The third delta function indicates the incompressibility condition. Remember that the volume of counterions is set as zero. The next two delta functions are the normalization conditions for f, g, and h. The last six delta functions are the constraint conditions that impose the sites (a_1, a_2, a_1c_1, a_2c_2, and a_1a_2) to lie on the A chain.

After the standard processing of SCFT, [66] we can obtain the mean field free energy from the partition function in Eq. (13). The resulting free energy is given by

$$\begin{aligned} \beta F = \int \mathrm{d}\mathbf{r}\Big[&-\sum_j\omega_j(\mathbf{r})\rho_j(\mathbf{r}) + \chi_{AB}\nu_A\nu_B\rho_A(\mathbf{r})\rho_B(\mathbf{r}) + \chi_{SA}\nu_S\nu_A\rho_S(\mathbf{r})\rho_A(\mathbf{r}) + \chi_{SB}\nu_S\nu_B\rho_S(\mathbf{r})\rho_B(\mathbf{r}) + \beta e\psi(\mathbf{r})\rho_e(\mathbf{r})\\ &- \frac{1}{2}\beta\varepsilon|\nabla\psi(\mathbf{r})|^2 + \eta(\mathbf{r})\left(\sum_j\rho_j(\mathbf{r})\nu_j - 1\right) - \big(\gamma_{f_1}(\mathbf{r})f_1(\mathbf{r}) + \gamma_{g_1}(\mathbf{r})g_1(\mathbf{r}) + \gamma_{h_1}(\mathbf{r})h_1(\mathbf{r})\big)\rho_{A_1}(\mathbf{r}) - \big(\gamma_{f_2}(\mathbf{r})f_2(\mathbf{r}) + \gamma_{g_2}(\mathbf{r})g_2(\mathbf{r})\\ &+ \gamma_{h_2}(\mathbf{r})h_2(\mathbf{r})\big)\rho_{A_2}(\mathbf{r}) + \alpha_1(\mathbf{r})\rho_{A_1}(\mathbf{r})(f_1(\mathbf{r}) + g_1(\mathbf{r}) + h_1(\mathbf{r}) - 1) + \alpha_2(\mathbf{r})\rho_{A_2}(\mathbf{r})(f_2(\mathbf{r}) + g_2(\mathbf{r}) + h_2(\mathbf{r}) - 1)\Big]\\ &- n_{p_1}\ln(VQ_{p_1}) + \ln(n_{p_1}!) - n_{p_2}\ln(VQ_{p_2}) + \ln(n_{p_2}!) - \sum_m VQ_m. \end{aligned} \tag{14}$$

Here, j represents all species in the system including monomers (A_1, A_2, B_1, and B_2), small ions (C_1 and C_2), and the solvent (S). $\rho_j(\mathbf{r})$ is the density field of species j, and $\omega_j(\mathbf{r})$ is the corresponding conjugated field. Note that the concentration of monomer A (B) includes the contributions from A_1 and A_2 (B_1 and B_2). Since we adopt the mean field approximation, the electrostatic contribution [the third line in Eq. (11)] comes from the inhomogeneous distribution of mean charge density ρ_e. Therefore, for a symmetric system with an equal amount of opposite charged blocks, its contribution should be zero due to the homogeneous charge density of $\rho_e(\mathbf{r}) = 0$. The electrostatic correlation effects are totally represented by the association of charged monomers with oppositely charged small ions or monomers. $\gamma_{f_1}(\mathbf{r})$, $\gamma_{f_2}(\mathbf{r})$, $\gamma_{g_1}(\mathbf{r})$, $\gamma_{g_2}(\mathbf{r})$, $\gamma_{h_1}(\mathbf{r})$, and $\gamma_{h_2}(\mathbf{r})$ are the corresponding conjugated fields for local fraction fields of the sites $f_1(\mathbf{r})$, $f_2(\mathbf{r})$, $g_1(\mathbf{r})$, $g_2(\mathbf{r})$, $h_1(\mathbf{r})$, and $h_2(\mathbf{r})$. $\eta(\mathbf{r})$ is a Lagrangian multiplier to ensure the incompressibility condition. $\alpha_1(\mathbf{r})$ and $\alpha_2(\mathbf{r})$ are the Lagrangian multiplier to ensure the normalization conditions for f, g, and h. Q_{p_1} and Q_{p_2} are the partition functions of single copolymer chains A_1B_1 and A_2B_2, respectively. They have the following expressions:

$$Q_{pi} = \frac{1}{V}\int \mathrm{D}\{\mathbf{R}^i(s)\}\exp\{-H^i_{cop}\}\delta(\mathbf{R}^{A_i}(N_{A_i}) - \mathbf{R}^{B_i}(N_{B_i})), \quad (15)$$

where H^i_{cop} satisfies

$$H^i_{cop} = \sum_{\alpha=A_i,B_i}\int_0^{N_\alpha} \mathrm{d}s\left[\frac{3}{2b^2}\left(\frac{\mathrm{d}\mathbf{R}^\alpha(s)}{\mathrm{d}s}\right)^2 + \omega_\alpha(\mathbf{R}^\alpha(s))\right], \quad (16)$$

where $i = 1, 2$. Q_m is the single molecule partition functions for species m. m includes all types of the small molecules and different reaction sites on A chains. They are given by

$$Q_{a_1} = \frac{1}{V}\int \mathrm{d}\mathbf{r}\exp(-\gamma_{f_1}(\mathbf{r}) - \beta\mu_{a_1})\rho_{A_1}(\mathbf{r}), \quad (17)$$

$$Q_{a_1c_1} = \frac{1}{V}\int \mathrm{d}\mathbf{r}\exp(-\gamma_{g_1}(\mathbf{r}) - \beta\mu_{a_1c_1})\rho_{A_1}(\mathbf{r}), \quad (18)$$

$$Q_{a_2} = \frac{1}{V}\int \mathrm{d}\mathbf{r}\exp(-\gamma_{f_2}(\mathbf{r}) - \beta\mu_{a_2})\rho_{A_2}(\mathbf{r}), \quad (19)$$

$$Q_{a_2c_2} = \frac{1}{V}\int \mathrm{d}\mathbf{r}\exp(-\gamma_{g_2}(\mathbf{r}) - \beta\mu_{a_2c_2})\rho_{A_2}(\mathbf{r}), \quad (20)$$

$$Q_{a_1a_2} = \frac{1}{V}\int \mathrm{d}\mathbf{r}\exp(-\gamma_{h_1}(\mathbf{r}) - \gamma_{h_2}(\mathbf{r}) - \beta\mu_{a_1a_2})\rho_{A_1}(\mathbf{r})\rho_{A_2}(\mathbf{r}), \quad (21)$$

$$Q_{C_1} = \frac{1}{V}\int \mathrm{d}\mathbf{r}\exp(-\omega_{C_1}(\mathbf{r}) - \beta\mu_{C_1}), \quad (22)$$

$$Q_{C_2} = \frac{1}{V}\int \mathrm{d}\mathbf{r}\exp(-\omega_{C_2}(\mathbf{r}) - \beta\mu_{C_2}), \quad (23)$$

$$Q_S = \frac{1}{V}\int \mathrm{d}\mathbf{r}\exp(-\omega_S(\mathbf{r}) - \beta\mu_S). \quad (24)$$

The self-consistent field (SCF) equations can be obtained by minimization of βF with respect to each fields appeared in Eq. (14). By taking functional derivatives of βF with respect to $\rho_j(\mathbf{r})$ and setting it equal to zero, the SCF equations about $\omega_j(\mathbf{r})$ is given by

$$\omega_{A_1}(\mathbf{r}) = \chi_{AB}\nu_A\nu_B\rho_B(\mathbf{r}) + \chi_{SA}\nu_S\nu_A\rho_S(\mathbf{r}) - \alpha_1(\mathbf{r}) + \nu_A\eta(\mathbf{r}) - 1, \quad (25)$$

$$\omega_{A_2}(\mathbf{r}) = \chi_{AB}\nu_A\nu_B\rho_B(\mathbf{r}) + \chi_{SA}\nu_S\nu_A\rho_S(\mathbf{r}) - \alpha_2(\mathbf{r}) + \nu_A\eta(\mathbf{r}) - 1, \quad (26)$$

$$\omega_{B_1}(\mathbf{r}) = \chi_{AB}\nu_A\nu_B\rho_A(\mathbf{r}) + \chi_{SB}\nu_S\nu_B\rho_S(\mathbf{r}) + \nu_B\eta(\mathbf{r}), \quad (27)$$

$$\omega_{B_2}(\mathbf{r}) = \chi_{AB}\nu_A\nu_B\rho_A(\mathbf{r}) + \chi_{SB}\nu_S\nu_B\rho_S(\mathbf{r}) + \nu_B\eta(\mathbf{r}), \quad (28)$$

$$\omega_{C_1}(\mathbf{r}) = z_{C_1}\beta e\psi(\mathbf{r}) + \nu_{C_1}\eta(\mathbf{r}), \quad (29)$$

$$\omega_{C_2}(\mathbf{r}) = z_{C_2}\beta e\psi(\mathbf{r}) + \nu_{C_2}\eta(\mathbf{r}), \quad (30)$$

$$\omega_S(\mathbf{r}) = \chi_{SA}\nu_S\nu_A\rho_A(\mathbf{r}) + \chi_{SB}\nu_S\nu_B\rho_B(\mathbf{r}) + \nu_S\eta(\mathbf{r}). \quad (31)$$

By equaling the functional derivatives of βF with respect to $\omega_j(\mathbf{r})$ to zero, we can obtain the SCF equations about $\rho_j(\mathbf{r})$,

$$\rho_{A_1}(\mathbf{r}) = \frac{n_{p_1}}{VQ_{p_1}}\int_0^{N_{A_1}} dsq_{A_1}(\mathbf{r},s)q^+_{A_1}(\mathbf{r},N_{A_1}-s), \quad (32)$$

$$\rho_{A_2}(\mathbf{r}) = \frac{n_{p_2}}{VQ_{p_2}}\int_0^{N_{A_2}} dsq_{A_2}(\mathbf{r},s)q^+_{A_2}(\mathbf{r},N_{A_2}-s), \quad (33)$$

$$\rho_{B_1}(\mathbf{r}) = \frac{n_{p_1}}{VQ_{p_1}}\int_0^{N_{B_1}} dsq_{B_1}(\mathbf{r},s)q^+_{B_1}(\mathbf{r},N_{B_1}-s), \quad (34)$$

$$\rho_{B_2}(\mathbf{r}) = \frac{n_{p_2}}{VQ_{p_2}}\int_0^{N_{B_2}} dsq_{B_2}(\mathbf{r},s)q^+_{B_2}(\mathbf{r},N_{B_2}-s), \quad (35)$$

$$\rho_{C_1}(\mathbf{r}) = \exp(-\omega_{C_1}(\mathbf{r}) - \beta\mu_{C_1}), \quad (36)$$

$$\rho_{C_2}(\mathbf{r}) = \exp(-\omega_{C_2}(\mathbf{r}) - \beta\mu_{C_2}), \quad (37)$$

$$\rho_S(\mathbf{r}) = \exp(-\omega_S(\mathbf{r}) - \beta\mu_S). \quad (38)$$

Here, $q_{A_1}(\mathbf{r},s)$ is the A_1-chain propagator and defined as the probability of finding the end monomer of the A_1 block of length s at point $\mathbf{r}$ with a free initial monomer. $q^+_{A_1}(\mathbf{r},s)$ is the probability of finding the end monomer of the A_1 chain of length s at $\mathbf{r}$, while the other end of the A_1 chain is connected to the whole B_1 block.[67] $q_{A_1}(\mathbf{r},s)$ and $q^+_{A_1}(\mathbf{r},s)$ satisfy the modified diffusion equations,

$$\frac{\partial q_{A_1}(\mathbf{r},s)}{\partial s} = \frac{b^2}{6}\nabla^2 q_{A_1}(\mathbf{r},s) - \omega_{A_1}(\mathbf{r})q_{A_1}(\mathbf{r},s), \quad (39)$$

$$\frac{\partial q^+_{A_1}(\mathbf{r},s)}{\partial s} = \frac{b^2}{6}\nabla^2 q^+_{A_1}(\mathbf{r},s) - \omega_{A_1}(\mathbf{r})q^+_{A_1}(\mathbf{r},s), \quad (40)$$

with the initial condition

$$q_{A_1}(\mathbf{r},0) = 1, q^+_{A_1}(\mathbf{r},0) = q_{B_1}(\mathbf{r},N_{B_1}). \quad (41)$$

The other propagators $q_\alpha(\mathbf{r}, s)$ and $q_\alpha^+(\mathbf{r}, s)$ ($\alpha = A_2, B_1, B_2$) have the similar definitions. Q_{p_1} and Q_{p_2} can then be simply evaluated by

$$Q_{p_i} = \frac{1}{V}\int d\mathbf{r} q_{A_i}^+(\mathbf{r}, N_{A_i}) = \frac{1}{V}\int d\mathbf{r} q_{B_i}^+(\mathbf{r}, N_{B_i}), \tag{42}$$

where $i = 1, 2$. With the same method, the remaining SCF equations can be obtained,

$$f_1(\mathbf{r}) = \exp(-\gamma_{f_1}(\mathbf{r}) - \beta\mu_{a_1}), \tag{43}$$

$$f_2(\mathbf{r}) = \exp(-\gamma_{f_2}(\mathbf{r}) - \beta\mu_{a_2}), \tag{44}$$

$$g_1(\mathbf{r}) = \exp(-\gamma_{g_1}(\mathbf{r}) - \beta\mu_{a_1c_1}), \tag{45}$$

$$g_2(\mathbf{r}) = \exp(-\gamma_{g_2}(\mathbf{r}) - \beta\mu_{a_2c_2}), \tag{46}$$

$$h_1(\mathbf{r}) = \exp(-\gamma_{h_1}(\mathbf{r}) - \gamma_{h_2}(\mathbf{r}) - \beta\mu_{a_1a_2})\rho_{A_2}(\mathbf{r}), \tag{47}$$

$$h_2(\mathbf{r}) = \exp(-\gamma_{h_1}(\mathbf{r}) - \gamma_{h_2}(\mathbf{r}) - \beta\mu_{a_1a_2})\rho_{A_1}(\mathbf{r}), \tag{48}$$

$$\gamma_{f_1}(\mathbf{r}) = \alpha_1(\mathbf{r}) + z_{A_1}\beta e\psi(\mathbf{r}), \tag{49}$$

$$\gamma_{f_2}(\mathbf{r}) = \alpha_2(\mathbf{r}) + z_{A_2}\beta e\psi(\mathbf{r}), \tag{50}$$

$$\gamma_{g_1}(\mathbf{r}) = \alpha_1(\mathbf{r}) + \nu_{C_1}\eta(\mathbf{r}), \tag{51}$$

$$\gamma_{g_2}(\mathbf{r}) = \alpha_2(\mathbf{r}) + \nu_{C_2}\eta(\mathbf{r}), \tag{52}$$

$$\gamma_{h_1}(\mathbf{r}) = \alpha_1(\mathbf{r}), \tag{53}$$

$$\gamma_{h_2}(\mathbf{r}) = \alpha_2(\mathbf{r}), \tag{54}$$

$$f_1(\mathbf{r}) + g_1(\mathbf{r}) + h_1(\mathbf{r}) = 1, \tag{55}$$

$$f_2(\mathbf{r}) + g_2(\mathbf{r}) + h_2(\mathbf{r}) = 1, \tag{56}$$

$$\sum_j \rho_j(\mathbf{r})\nu_j = 1, \tag{57}$$

$$\beta e\nabla^2\psi(\mathbf{r}) + 4\pi l_B\rho_e(\mathbf{r}) = 0. \tag{58}$$

Here, l_B in Eq. (58) is the Bjerrum length and is defined as $l_B = e^2/(\varepsilon k_B T)$.

Equations (25)–(38) and (43)–(58) constitute a closed set of SCF equations for our system and can be solved numerically. In Eqs. (36)–(38) and (43)–(48), the constant prefactors $\exp(-\beta\mu_{C_1})$, $\exp(-\beta\mu_{C_2})$, $\exp(-\beta\mu_S)$, $\exp(-\beta\mu_{a_1})$, $\exp(-\beta\mu_{a_2})$, $\exp(-\beta\mu_{a_1c_1})$, $\exp(-\beta\mu_{a_2c_2})$, and $\exp(-\beta\mu_{a_1a_2})$ are used to define the bulk conditions $\rho_{C_1}^b$, $\rho_{C_2}^b$, ρ_S^b, f_1^b, f_2^b, g_1^b, g_2^b, and h^b, respectively. $\rho_{C_1}^b$ and $\rho_{C_2}^b$ are equal to bulk salt concentration ρ_{salt}. In addition, the three equilibrium constants can be defined as

$$K_{a_1c_1} = \exp[-\beta(\mu_{a_1c_1} - \mu_{a_1} - \mu_{C_1})] = \frac{g_1^b}{f_1^b\rho_{C_1}^b}, \tag{59}$$

$$K_{a_2c_2} = \exp[-\beta(\mu_{a_2c_2} - \mu_{a_2} - \mu_{C_2})] = \frac{g_2^b}{f_2^b\rho_{C_2}^b}, \tag{60}$$

$$K_{aa} = \exp[-\beta(\mu_{a_1a_2} - \mu_{a_1} - \mu_{a_2})] = \frac{h^b}{f_1^b f_2^b}, \tag{61}$$

which are the measurements of the strength of ion pair formation. K_{aa} reflects the binding strength between oppositely charged monomers from A blocks. $K_{a_1c_1}$ (or $K_{a_2c_2}$) reflects the binding strength between monomer A_1 (or A_2) and small ion C_1 (or C_2). For simplicity, we further assume $K_{a_1c_1} = K_{a_2c_2} = K_{ac}$. Thus, parameters K_{aa} and K_{ac} determine the strength of electrostatic correlations. In addition, we define the total concentration of small ions C_1 and C_2 as $\rho_{C_1}^{\text{total}} = \rho_{C_1}(\mathbf{r}) + g_1(\mathbf{r})\rho_{A_1}(\mathbf{r})$ and $\rho_{C_2}^{\text{total}} = \rho_{C_2}(\mathbf{r}) + g_2(\mathbf{r})\rho_{A_2}(\mathbf{r})$, for the small ions are composed of the part binding with polymer chains and the part that are dissociated from salts.

With given parameters, after solving the set of SCF equations, one obtain the free energy density for a specified ordered phase. The ordered structures considered in this article include the lamellar phase (L), hexagonal cylinder phase (H), and body-centered cubic phase (B). When dealing with two or three dimensional structures (H and B), we use the unit-cell approximation to reduce the calculation.[68] We extract unit cells from the multi-dimensional structures and approximate them to a circle (H phase) or a sphere (B phase). The free energy density at equilibrium is obtained by minimizing it with respect to the size of the unit cell. The phase diagram then can be constructed by comparing the free energy densities for different ordered phases, and the morphology with the lowest energy density is chosen as the equilibrium phase. It is important to note that our model ignores the possibility of gelation, which is created by the strong binding between oppositely charged polymer monomers. In principle, the polymer conformational entropy and the electrostatic correlations need to be accounted for in accord with these polyion cross-linking.[48] The formation of gelation network within the complexed A-rich region involves in a rather complicated process, and a complete treatment to the charged polymer cluster is not easy. In this work, we lay that complex problem aside and simply focus on the binding of ion pairs. Our above method is a primary starting for current coacervate-driven self-assembly accompanied with ion pairs. The later calculations indicate that our model gives a good prediction for the experimental results of block polyelectrolytes with high linear charge density.

III. RESULTS AND DISCUSSIONS

In this study, we emphasize the importance of the binding effect between positively charged species and negatively charged species. The dielectric effects[69] and the excluded volume interactions involving counterions are omitted. In order to highlight the role of the electrostatic effect, some parameters are fixed in the calculations. We set b as the length unit. The degrees of polymerization of two oppositely charged polymer chains are fixed as $N_1 = N_2 = 100$. Both of the two chains are set to have the same bulk concentration. In addition, the total volume fraction of the polymer is denoted by ϕ_p. The volume of monomers and solvents is assumed to be the same value, $v_A = v_B = v_S = b^3$. The small ions are point-like charges with the volume of zero for C_1 and C_2. The charged monomers and small ions are monovalent with $z_{A_1} = 1.0$, $z_{A_2} = -1.0$, $z_{C_1} = -1.0$, and

z_{C_2} = 1.0. The Bjerrum length l_B is 0.7, which is a typical value for water solution with b = 1 nm. The Flory–Huggins interaction parameters between the solvent and the monomers (χ_{SA} and χ_{SB}) are zero.

A. Effect of charge association

1. Effect of binding strength between oppositely charged blocks

K_{aa} reflects the binding strength between two oppositely charged A blocks. A larger K_{aa} corresponds to a stronger binding strength. Taking the lamellar phase with ϕ_p = 0.5 as an example, we study the effect of K_{aa} on its structures. The results are shown in Fig. 2. In Fig. 2(a), the free energy density at equilibrium decreases monotonically with increasing K_{aa}, indicating that the binding of charged monomers on two blocks improve the stability of ordered phase. The domain size also increases monotonically as K_{aa} increases, showing a more significant effect on phase separation. As K_{aa} increases, the concentration of the A_1 monomer increases in the A-rich domain and decreases in the B-rich domain [Fig. 2(b)], leading to a much narrower A–B interface. The concentration distribution of mobile small ion C_1 shows a more complicated relationship to K_{aa} [Fig. 2(c)]. The concentration of C_1 distributed in the B-rich domain decreases with increasing K_{aa}, resulting from the decrease in A_1 monomer concentration. However, the concentration of C_1 distributed in the A-rich domain changes in a non-monotonic way, first increasing and then decreasing as K_{aa} increases. This phenomenon is caused by the combined influence of the increasing concentration of A_1 and the decreasing fraction of g_1 (we will discuss it below). It is also noted that the distribution of salt ions here is different from the result of Ong[60] (salt ions prefer to be in the neutral B block, not the charged A block). We attribute this disparity to the omission of excluded volume interactions with salt ions in our model.

For each charged site on the chain, it can be paired either with the oppositely charged small ions or the monomers from another oppositely charged chain. Apparently, the two kinds of ion pairing compete with each other. Such competitive relationship can be observed from the distribution of ion pairs. For example, the A_1 monomer can be paired with small ion C_1 or with monomer A_2. Figures 2(d)–2(f) give the spatial distribution for the fraction of different sites on A_1 chains. f_1 is the fraction for non-paired charged A_1 monomers. g_1 is the fraction of A_1 monomers neutralized by the small ion C_1 (i.e., ion pair $[A_1C_1]$) and h_1 is that neutralized by A_2 monomers (i.e., ion pair $[A_1A_2]$). Generally, the f_1 value in the B-rich domain is larger than that in the A-rich domain [Fig. 2(d)], implying that the A blocks distributed in the B-rich domain are easier to be in the ionized state since the charged species in the B-rich domain are less. The value of g_1 in the B-rich domain is also larger than that in the A-rich domain [Fig. 2(e)], indicating that the A_1 monomer in the B-rich domain is easier to bind with small ions. Meanwhile, the concentration of small ion C_1 is lesser in the B-rich domain [Fig. 2(c)]. Considering the small amount of the A block

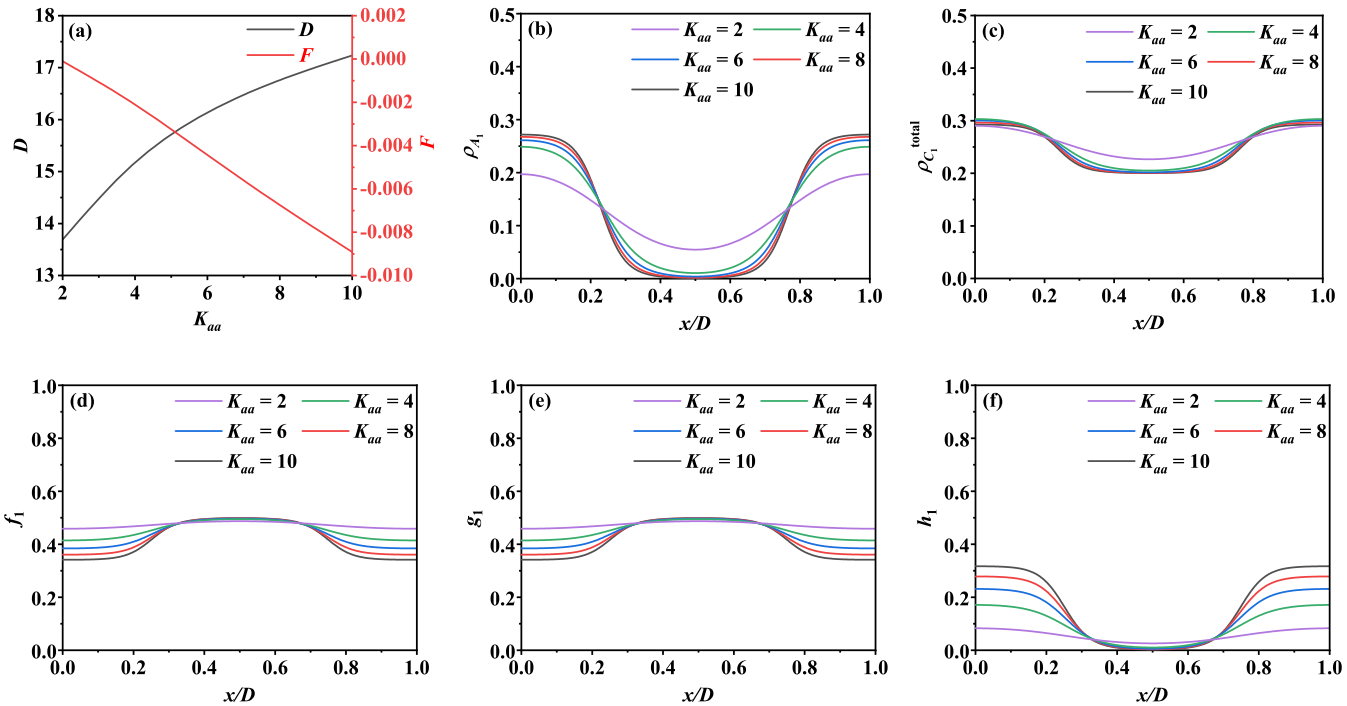

FIG. 2. The influence of K_{aa} on the structure for a typical lamellar phase with χ_{AB} = 0.12, $f_{A_1} = f_{A_2}$ = 0.5, ϕ_p = 0.5, ρ_{salt} = 0.20, and K_{ac} = 5. (a) Domain size (D) and free energy (F). (b) Concentration distribution of monomer A_1 (ρ_{A_1}). (c) Concentration distribution of small ion C_1 ($\rho_{C_1}^{total}$). (d) The distribution of charged fraction for the A_1 block (f_1). (e) The distribution of the fraction of the A_1 block associated with small ion C_1 (g_1). (f) The distribution of the fraction of the A_1 block associated with the A_2 block (h_1).

in the B-rich domain, such a phenomenon results from lack of competition from A_2. From Fig. 2(f), the ion pairs formed from A_1 and A_2 blocks are mainly distributed in the A-rich domain, which is a natural result due to the high concentration of the A block in this domain. Moreover, in the A-rich domain, the improvement of the K_{aa} value increases the value of h_1 but decreases the value of f_1 and g_1, implying that many charged sites and C_1-neutralized sites are replaced by the enhanced combination between oppositely charged monomers on two A blocks. On the other hand, the values of f_1, g_1, and h_1 in the B-rich domain remain nearly constant due to the lack of A monomers here.

For the neutral block copolymer system, the driving force to the microphase separation is the immiscibility between different blocks, i.e., a large enough Flory–Huggins interaction parameter χ_{AB}.[70] For block polyelectrolytes with opposite charges, the electrostatic attraction via pairing of charged blocks may play a key role in driving phase separation. In terms of our model, microphase separation can still occur even when the immiscibility is low. Figure 3(a) plots the domain size and free energy of the lamellar phase as a function of χ_{AB} at $K_{aa} = 1 \times 10^{-5}$. The rather small value of K_{aa} corresponds to a system without pairing between A_1 and A_2. As χ_{AB} decreases, the free energy increases and gradually approaches zero accompanied by a decrease in the domain size. The order–disorder transition point is $\chi_{AB} \simeq 0.211$ in such a χ_{AB}-driven system (the ordered phase corresponds to a negative free energy of the assembled systems). With χ_{AB} decreasing, the concentration distribution of monomer A_1 also becomes more homogeneous, and the effective degree of microphase separation is reduced [Fig. 3(b)]. In case of strong binding between A_1 and A_2 with $K_{aa} = 10$, the microphase separation can still be observed even if χ_{AB} drops to zero. In other words, phase separation occur without incompatibility interaction. The strong charge correlation (charge paring) provides a driving force for phase separation. It can also be seen from Fig. 3(d) that there is little change in the concentration distribution of monomer A_1 in such a charge correlation-driven system when χ_{AB} changes from 0.20 to zero. This strong binding between A_1 and A_2 results in effective strong segregation between A and B blocks. In addition, the domain size D is proportional to χ_{AB} for the small χ_{AB} value.

2. Effect of binding between charged monomers on chains and small ions

The binding strength K_{ac} between charged monomers on chains and small ions may play an important role in determining the self-assembled structures. In terms of its definition, a larger value of K_{ac} corresponds to the larger binding strength. A smaller K_{ac} value indicates a weak association between the charged monomer and small ions, which corresponds to polyelectrolytes bearing stronger ionic groups (low pK_a value) and larger degree of ionization. Figure 4 gives an example on the effect of K_{ac} on a lamellar phase. Compared with K_{aa}, K_{ac} shows an opposite effect. In Fig. 4(a), free energy density increases as K_{ac} increases, accompanied by a reduction of the domain size. The free energy density is nearly zero when K_{ac} is large enough, which is close to the result of the homogeneous phase. As a consequence, increasing K_{ac} has a tendency to prevent

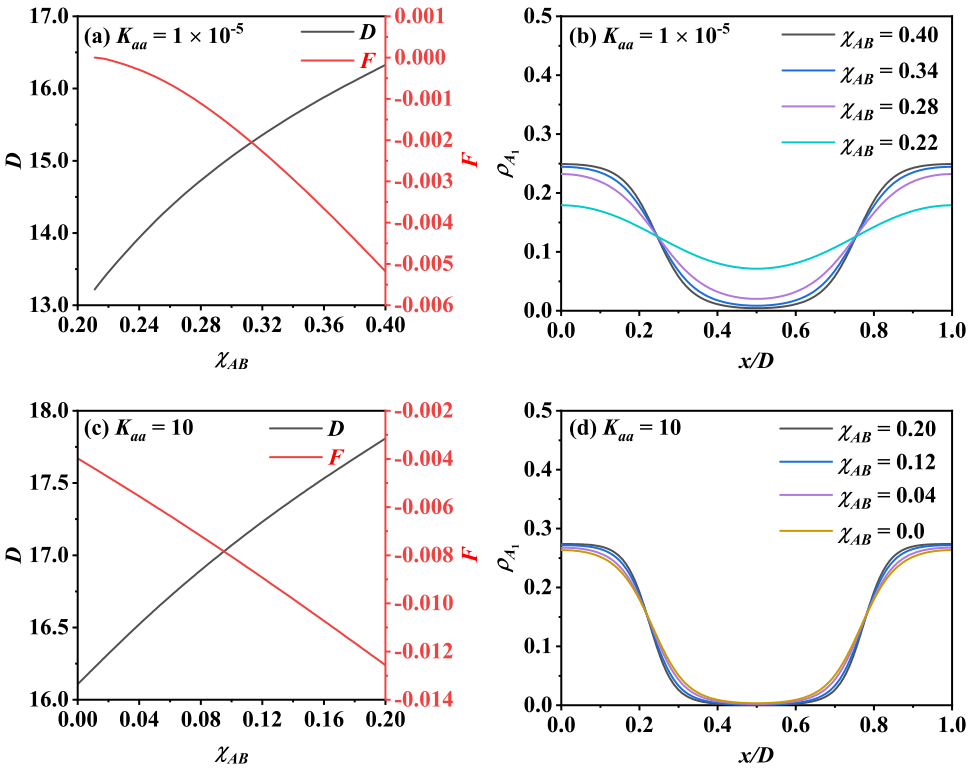

FIG. 3. The effect of χ_{AB} on the structure of a lamellar phase with $f_{A_1} = f_{A_2} = 0.5$, $\phi_p = 0.5$, $\rho_{salt} = 0.20$, and $K_{ac} = 5$. (a) Domain size (D) and free energy (F) at $K_{aa} = 1 \times 10^{-5}$. (b) Concentration distribution of monomer A_1 at $K_{aa} = 1 \times 10^{-5}$ for various χ_{AB}. (c) Domain size (D_0) and free energy (F) at $K_{aa} = 10$. (d) Concentration distribution of monomer A_1 at $K_{aa} = 10$ for various χ_{AB}.

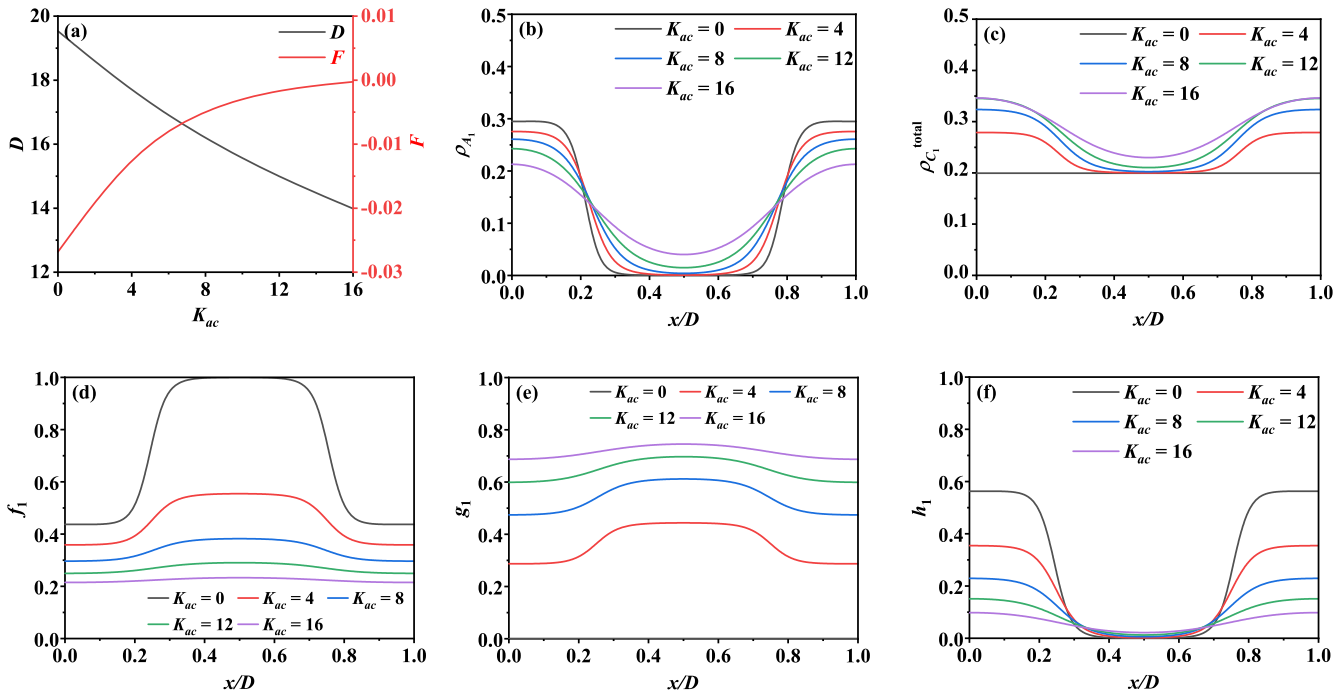

FIG. 4. The influence of K_{ac} on the structure of a lamellar phase with χ_{AB} = 0.12, $f_{A_1} = f_{A_2}$ = 0.5, ϕ_p = 0.5, ρ_{salt} = 0.20, and K_{aa} = 10. (a) Domain size (D) and free energy (F). (b) Concentration distribution of monomer A_1 (ρ_{A_1}). (c) Concentration distribution of small ions C_1 ($\rho_{C_1}^{total}$). (d) The distribution of the charged fraction for the A_1 block (f_1). (e) The distribution of the fraction of the A_1 block associated with small ions C_1 (g_1). (f) The distribution of the fraction of the A_1 block associated with the A_2 block (h_1).

microphase separation, which is also confirmed by the more homogeneous concentration distribution of A_1 with increasing K_{ac} [see Fig. 4(b)]. The concentration of small ion C_1 also rises in the whole space, coming from the stronger combination of small ions and charged blocks [see Fig. 4(c)].

The inhibitory effect of increasing K_{ac} on phase separation is accomplished by suppressing the binding between oppositely charged A blocks. As mentioned before, there is a competitive binding with A_1 monomers between small ions C_1 and charged monomers A_2. When K_{ac} is very small, the fraction of charged sites from A_1 and A_2 is dominant within the B-rich domain ($f_1 \simeq 1$). In this case, the concentration of charged A blocks is very small so that the association probability between A_1 and A_2 is also low and A monomers tend to be in the naked charge state. With the increase in K_{ac}, the fraction f_1 drops off, indicating that the number of charged A_1 monomers is reduced [Fig. 4(d)]. On the other hand, it leads to an increase in the number of ion pairs [A_1C_1], thus causing the increase in the g_1 fraction [Fig. 4(e)], which is a reasonable result. For the h_1 fraction in Fig. 4(f), the formation of ion pairs [A_1A_2] is suppressed under the effect of K_{ac}, leading to the reduction of h_1. In addition, when K_{ac} becomes large enough, f_1, g_1, and h_1 curves become flat in the whole space.

In brief summary, K_{aa} and K_{ac} have opposite effects on phase separation. An increase in K_{aa} can promote phase separation since the binding between opposite charges on two blocks is the main driving force for phase separation. In contrast, an increase in K_{ac} inhibits phase separation, indicating that the binding between charged monomers on chains and small ions is unfavorable for phase separation. Such an inhibitory effect of K_{ac} results from the preferable combination between one charged monomer with small ions instead of that with oppositely charged monomers on another chains. In addition, we note here that the results of the A_2 block are the same as that of the A_1 block because of the symmetry in our system. Experimentally, Hunt *et al.*[39] examined the influence of polyelectrolyte pK_a on the coacervate-driven triblock system. They changed the ionic groups on the polyelectrolyte chains and studied the properties of formed hydrogels. They found that the mixing solutions of copolyelelctrolytes bearing weaker ionic groups (strong binding with counterions) produced a viscous fluid. However, mixing of the copolyelectrolytes with the strongest ionic groups (corresponding to a small K_{ac} value in our model) formed the most stable, mechanically resilient gels at the lowest polymer concentration. Their results provide direct evidence for the role of charge correlation in our model.

B. Effect of salt

It is well known that an increase in salt concentration produces stronger screening for the electrostatic interactions between charges, thus it decreases driving force for coacervation and inhibits phase separation.[39,60,64] This phenomenon can be observed in our model, as shown in Fig. 5. Here, the effect of salt concentration for the lamellar phase with a polymer concentration of ϕ_p = 0.5 is considered. As the small ions are assumed to be point-like charges without volume,

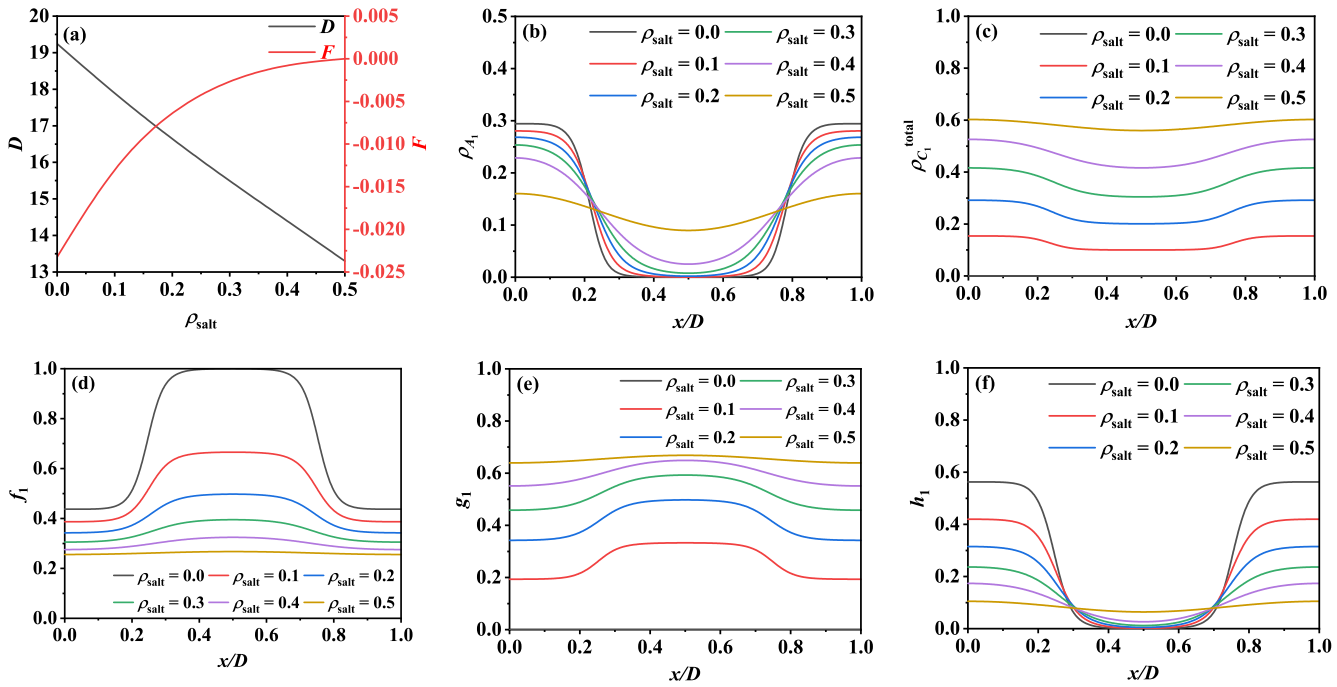

FIG. 5. The effect of salt concentration for a typical lamellar phase with $\chi_{AB} = 0.05$, $f_{A_1} = f_{A_2} = 0.5$, $\phi_p = 0.5$, $K_{ac} = 5$, and $K_{aa} = 10$. (a) Domain size (D) and free energy (F). (b) Concentration distribution of monomer A_1 (ρ_{A_1}). (c) Concentration distribution of small ions C_1 ($\rho_{C_1}^{total}$). (d) The distribution of the charged fraction for the A_1 block (f_1). (e) The distribution of the fraction of A_1 monomers binding with small ion C_1 (g_1). (f) The distribution of the fraction of A_1 monomers binding with A_2 monomers (h_1).

the excluded volume interactions involving counterions are ignored here. The values of K_{ac} and K_{aa} are set to be 5 and 10, respectively, which are modest values for phase separation. The free energy shows a monotonically increased dependence on salt concentration, and the domain size drops quickly [Fig. 5(a)]. It is interesting that the domain size is almost a linear function of salt concentration, which is in good agreement with the experiment results.[40] The flattening of ρ_{A_1} upon adding salts is also observed [Fig. 5(b)]. The concentration of small ions C_1 increases as salt concentration increases as it should be [Fig. 5(c)]. Meanwhile, the gradient of ρ_{C_1} in the AB two-phase interface disappears gradually.

The screening effect of salt on the charges from the polymer chain is evident here. It is need to be pointed out that the screening effect of added salt is achieved by enrichment of small ions around pure charges and weakening of the electric field. In our model, the mean field treatment in fact predict an almost homogeneous electric potential ψ over space as the result of two symmetric oppositely charged copolymers. Therefore, the weakening effect of electric field from salts on pure charges (charged sites) is not included explicitly in our model. Instead, the screening effect is embodied by reducing considerably the pairing of $[A_1A_2]$. The detailed information about the spatial distribution of ion pairs is shown in Figs. 5(d)–5(f). By adding more salts into the system, the value of f_1 decreases, while the value of g_1 increases, indicating more charged A_1 monomers are paired with small ions. The h_1 value in the A-rich domain drops with increasing salt concentration, demonstrating the enhanced replacement of $[A_1A_2]$ pairing by $[A_1C_1]$ pairing. However, the h_1 value in the B-rich domain increases slightly with salt concentration, implying the combination of two kinds of charged monomers is enhanced. This non-trivial phenomenon may be due to the obvious increase in charged A_1 and A_2 monomers in B-rich regions, which enhance, in turn, the association probability between them. The three distributions of f_1, g_1, and h_1 also become flatter with increasing salt concentration. The effect of salt concentration is similar to that of K_{ac}. The main difference between the two factors is that f_1, g_1, and h_1 fractions have the modest variation and will not decrease (or increase) to 0 (or 1) when adding enough salt ions. Although the above results are for the lamellar phase with $\phi_p = 0.5$, the equilibrium structures of both polymer melts and other self-assembled morphologies show similar variation tendency with parameters, as shown in Figs. 2–5.

C. Phase diagram

In this part, we construct the phase diagrams as a function of salt concentration (ρ_{salt}) and polymer concentration (ϕ_p) in order to show the influence of binding strength and composition. Then, the theoretical predictions are compared with the experimental results. For ordered H (or B) phases, both the A-rich domain and B-rich domain can form a cylinder (or sphere) core. Thus, we mark the two cases as H1 and H2 (or B1 and B2), respectively. The disorder phase is denoted by Dis. The Flory–Huggins parameter between A and B

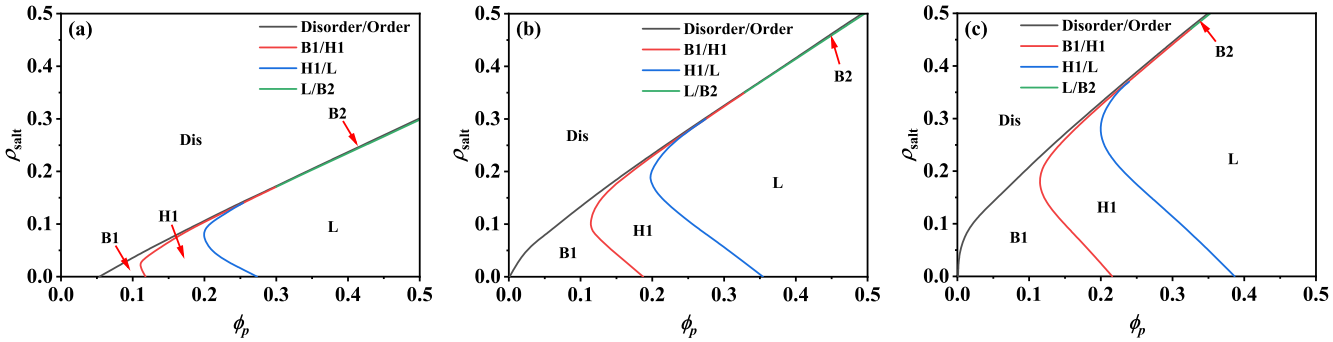

FIG. 6. Salt concentration (ρ_{salt}) vs polymer concentration (ϕ_p) phase diagram with increasing the association parameter K_{aa} between oppositely charged monomers at χ_{AB} = 0.05, $f_{A_1} = f_{A_2} = 0.5$, and K_{ac} = 5.0. (a) K_{aa} = 5.0, (b) K_{aa} = 10.0, and (c) K_{aa} = 15.0. Dis denotes the disordered (homogeneous) phase, B1 denotes the body-centered cubic phase with A blocks forming the sphere core, and H1 denotes the hexagonal cylinder phase with A blocks forming the cylinder core. L denotes the lamellar phase, and B2 denotes the body-centered cubic phase with B blocks forming the sphere core.

blocks is set as χ_{AB} = 0.05, which represents a miscible system for neutral diblock copolymers.

1. Effect of K_{aa} on phase diagram

The effect of K_{aa} on the phase diagram has been shown in Fig. 6. f_{A_1} and f_{A_2} are chosen to be 0.5, corresponding to a symmetric polymer with the same length of A and B blocks. K_{ac} is chosen to be 5.0, corresponding to a moderate strength for the combination of small ions and charged monomers. In each phase diagram, four ordered structures, including B1, H1, L, and B2, are observed at high ϕ_p, where the electrostatic interaction is strong enough to drive the phase separation. The main feature of phase behavior in our model is similar to the transfer matrix theory based results from the work of Ong and Sing[60] although they do not consider the three dimensional structures. At low salt concentration ρ_{salt}, the phase changes following the sequence of Dis, B1, H1, and L with increasing the polymer concentration. Such transition order has been verified in some experimental results.[27,64] Increasing polymer concentration enhances the association between oppositely charged monomers, effectively leading to a larger immiscibility between A and B blocks. At the same time, adding more salt ions may result in ordered to disordered phase transition. The variation of K_{aa} from 5 to 15 does not change the shape of the phase diagram, instead it influences the domain area of each ordered phase. In general, the windows of all ordered phases are enlarged as K_{aa} increases, indicating that K_{aa} has the tendency of promoting phase separation. The effect of K_{aa} is also more obvious at the high ϕ_p region here.

The salt-induced phase transition is more complicated. Take Fig. 6(b) as an example. At ϕ_p = 0.12, a transition from B1 to H1 then to B1 can be observed when increasing salt concentration. The salt-induced re-entrant phenomenon is interesting, and it has been found in some experiments.[71] The equilibrium phase results from the subtle balance between different factors. With the initial increase in salt ions, the translational entropy of mobile small ions probably plays an important role, leading to the B1–H1 or H1–L transition for seeking larger translational entropy for small ions confined inside condensed core. On the other hand, further increasing salt ions produces stronger screening effect by decreasing the number of A1–A2 ion pairs. Effectively, the immiscibility between A and B blocks is reduced and drives the transition to phases with larger curvature, a similar influence as decreasing for neutral block copolymers. However, at ϕ_p = 0.1, no phase transition can be observed when salt concentration is changed. The phenomenon that salt-induced morphological change is absent for the B phase has been observed in the experimental results of Hunt.[39] Another interesting feature is that at high ϕ_p and ρ_{salt}, there exists a rather narrow window of the B2 phase in the middle of the L phase and disordered phase. In the results of Ong and Sing for a similar system, they observed a wide window for the H2 phase.[60] The presence of a narrow region of the B2 phase in our model indicates the neutral B blocks aggregating to form sphere or cylinder are very disadvantageous in this case.

2. Effect of K_{ac} on phase diagram

Figure 7 gives the effect of K_{ac} on the phase diagram at $f_{A_1} = f_{A_2} = 0.5$ and K_{aa} = 10. Similar to K_{aa}, the variation of K_{ac} does not change the main character of the phase diagram, and four ordered phases (B1, H1, L, and B2) are observed. As mentioned above, increasing K_{ac} has been proved to suppress the phase separation. Here, the range of each ordered phase shrinks as K_{ac} increases, and the phase transition boundaries seem to be compressed along the Y axis. Low salt concentration is required in order to induce phase separation. Moreover, it is observed that the transition boundaries of phases in the salt-free case ($\rho_{salt} = 0$) are nearly independent of K_{ac} values. Therefore, one can infer that in the absence of salt ions, the binding strength between counterions and charged monomers hardly affects the phase morphology even if it is very strong. Considering the similarity between these phase diagrams, we speculate that the salt concentration ρ_{salt} and binding constant K_{ac} are not independent in the case of strong ion paring of $[A_1A_2]$. To prove this point, we plot the phase diagrams with different K_{ac} values into one figure with effective salt concentration $\rho_{salt}K_{ac}$ as the Y coordinate. Figure 7(d) displays the result. It is found that these diagrams can be normalized, which means that the parameters $\rho_{salt}K_{ac}$ and ϕ_p are the two independent variables determining the phase behavior of coacervate-driven self-assembly of block polyelectrolytes.

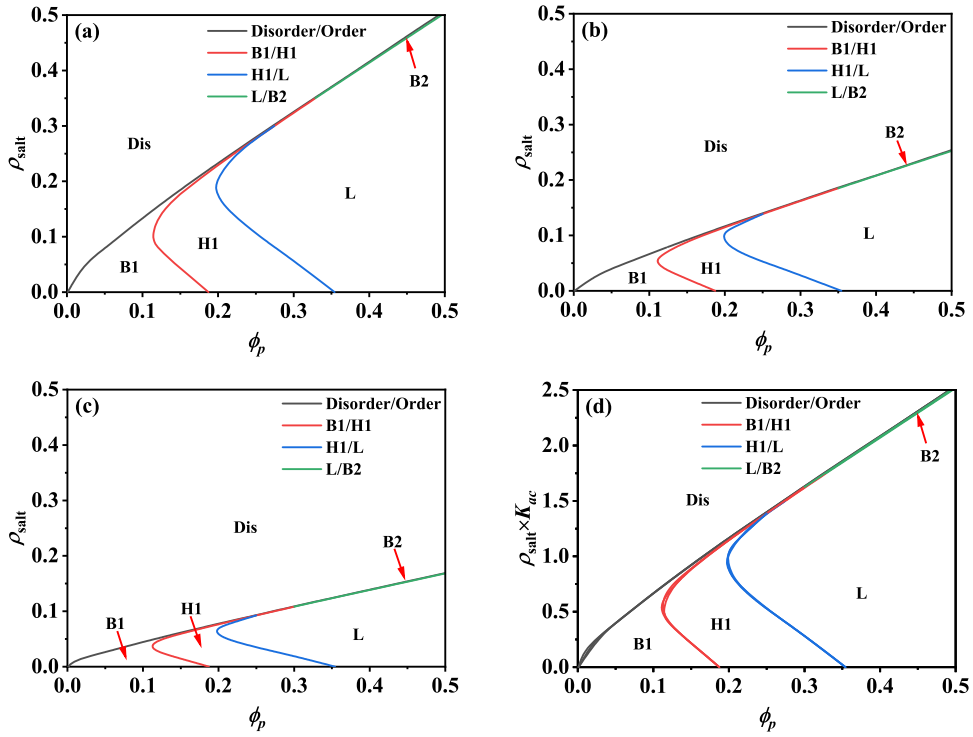

FIG. 7. The effect of K_{ac} on the phase diagram at χ_{AB} = 0.05, $f_{A_1} = f_{A_2}$ = 0.5, and K_{aa} = 10. (a) K_{ac} = 5.0, (b) K_{ac} = 10.0, and (c) K_{ac} = 15.0. Dis, B1, H1, L, and B2 denote the same phases as in Fig. 6. (d) The normalized phase diagram in $\rho_{salt} \times K_{ac}$ vs ϕ_p parameter space in terms of Figs. (a)–(c). These figures can be cast into a normalized phase diagram.

3. Effect of f_A on phase diagram

The compositions of the A block f_{A_1} and f_{A_2} play an important role in determining the self-assembled structures of block copolyelectrolytes. We study how the phase diagram changes with the compositions. We further assume $f_{A_1} = f_{A_2} = f_A$, indicating that the two copolymers are the same except for the charge sign. K_{ac} and K_{aa} are chosen to be 5.0 and 10.0, respectively. Three compositions f_A = 0.3, 0.5, 0.7 are used. The corresponding results are shown in Fig. 8. It can be seen that f_A has considerable influence on the phase diagram.

When the A block is a minor component with f_A = 0.3 [Fig. 8(a)], only two ordered phases B1 and H1 are observed. In addition, the increase in polymer concentration or decrease in salt concentration can lead to the phase transition from the Dis phase to the B1 phase and then to the H1 phase within the parameter space we considered. It is attributed to the enhanced electrostatic correlations. In the case of f_A = 0.5 [Fig. 8(b)], the order–disorder phase transition boundary shifts leftward due to the improved charged block ratio on copolymer chains. The range of the B1 phase and H1 phase is compressed followed by the appearance of the L phase. When f_A is increased to 0.7, the order–disorder phase transition boundary shifts downward, implying that the stability of the ordered phase is decreased. Therefore, the close ratio of A and B blocks is most conducive to phase separation. In addition, Fig. 8(c) shows that the window of the B2 phase is significantly enlarged and the H2 phase appears for the first time. Increasing polymer concentration (ϕ_p)

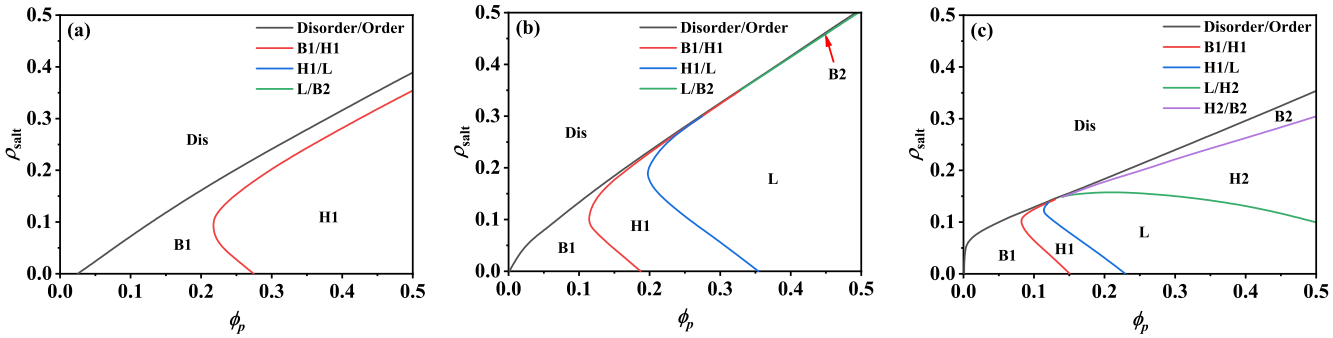

FIG. 8. The phase diagram at χ_{AB} = 0.05, K_{ac} = 5.0, and K_{aa} = 10.0 with varying composition f_A. (a) f_A = 0.3, (b) f_A = 0.5, and (c) f_A = 0.7. D, B1, H1, L, and B2 denote the same phases as in Fig. 6. H2 denotes the hexagonal cylinder phase with B blocks forming the cylinder core.

accompanied with adding more salt ions may induce the following phase transition: B1 → H1 → L → H2 → B2. The transition sequence is in analogy to the phase behavior of standard block copolymers when the ratio of the charged block is changed.[67,70] The polymer concentration plays a similar role as the composition of neutral diblock copolymer, while salt ions play a similar role as temperature. As for the boundaries of the order–order transition, the boundary shifts to low ϕ_p in a general trend. Finally, our results about the effect of f_A on the phase diagram for hexagonal and lamellar phases are somewhat similar to those of Ong and Sing using transfer matrix theory, [60] reflecting the reliability of our results.

We emphasis that the phase diagram in Fig. 8(a) is qualitatively comparable with the experimental results given by Krogstad *et al.*, [41] where only the B1 phase and H1 phase are observed under the usage of copolymer with $f_A < 0.4$. Although the precise comparison is difficult, the B1–H1 transition occurs at $\phi_p \simeq 0.3$ for salt-free solutions, which is very close to our prediction. In addition, in a recent article by Kim *et al.*, [71] their phase diagram shows far more compelling agreements with our calculational results, although what they studied is a triblock copolymer system.

IV. CONCLUSION

In summary, we have developed a new model to study the phase behavior of coacervate-driven self-assembly of the block polyelectrolyte system. The feature of our model is the introduction of reversible ions binding between oppositely charged species. The phase behavior of the system is determined to a large extent by two binding strength parameters K_{ac} and K_{aa}. There is a competition between these two binding modes. We have proved the opposite effects of K_{ac} and K_{aa} on phase separation. The increase in K_{aa} promotes the microphase separation, while the increase in K_{ac} suppresses the phase separation. In other words, the binding between oppositely charged monomers on chains is advantageous to phase separation, while the binding between charged monomers and small ions is disadvantageous. Our model predicts the existence of phase separation in the case of the low Flory–Huggins parameter. Adding salt ions will produce electrostatic screening by inhibiting the ion pairs between charged blocks and then decrease the tendency of phase separation.

Phase diagrams as a function of salt concentration and polymer concentration have been constructed, and three phase structures including the lamellar phase, hexagonal cylinder phase, and body-centered cubic phase are incorporated into the phase diagram. Increasing K_{aa} will increase the range of ordered phases. On the contrary, with strong monomer–monomer binding, the increase in K_{ac} results in the shrink of ordered phases. In this case, the product of salt concentration and K_{ac} constitutes a separated controlling parameter. Increasing the volume fraction of charged A blocks will lead to the appearance of more ordered phases. The salt concentration plays an analogous role to temperature for neutral block copolymer self-assembly. Our results are qualitatively in good agreement with the existing experimental literature.[27,39,41,64] Using our model, one can obtain the information about the spatial distribution of ion pairs, which is helpful to understand the self-assembled nanostructures. Our method is easy to be extended to other block polyelectrolyte systems with moderate or high linear charge density. The above results based on ion pairs give an in-depth understanding of phase separation for coacervate-driven self-assembly and provide a guidance for the experimental design of nanomaterials.

ACKNOWLEDGMENTS

The authors are grateful for the financial support provided by the National Natural Science Foundation of China (NSFC) (Grant Nos. 22073002, 21674005, and 21634001).

DATA AVAILABILITY

The data that support the findings of this study are available from the corresponding author upon reasonable request.

REFERENCES

[1] H. G. B. de Jong and H. R. Kruyt, "Coacervation (partial miscibility on colloid systems) (preliminary communication)," Proc. R. Acad. Amsterdam **32**, 849–856 (1929).
[2] A. B. Marciel, E. J. Chung, B. K. Brettmann, and L. Leon, "Bulk and nanoscale polypeptide based polyelectrolyte complexes," Adv. Colloid Interface Sci. **239**, 187–198 (2017).
[3] E. Spruijt, A. H. Westphal, J. W. Borst, M. A. Cohen Stuart, and J. van der Gucht, "Binodal compositions of polyeleetrolyte complexes," Macromolecules **43**, 6476–6484 (2010).
[4] H. Yoon, E. J. Dell, J. L. Freyer, L. M. Campos, and W.-D. Jang, "Polymeric supramolecular assemblies based on multivalent ionic interactions for biomedical applications," Polymer **55**, 453–464 (2014).
[5] W. C. Blocher and S. L. Perry, "Complex coacervate-based materials for biomedicine," Wiley Interdiscip. Rev.: Nanomed. Nanobiotechnol. **9**, 1442 (2017).
[6] E. Kizilay, A. B. Kayitmazer, and P. L. Dubin, "Complexation and coacervation of polyelectrolytes with oppositely charged colloids," Adv. Colloid Interface Sci. **167**, 24–37 (2011).
[7] S. L. Perry, Y. Li, D. Priftis, L. Leon, and M. Tirrell, "The effect of salt on the complex coacervation of vinyl polyelectrolytes," Polymers **6**, 1756–1772 (2014).
[8] J. Lou, S. Friedowitz, J. Qin, and Y. Xia, "Tunable coacervation of well-defined homologous polyanions and polycations by local polarity," ACS. Cent. Sci. **5**, 549–557 (2019).
[9] Z. Ou and M. Muthukumar, "Entropy and enthalpy of polyelectrolyte complexation: Langevin dynamics simulations," J. Chem. Phys. **124**, 154902 (2006).
[10] D. Priftis, N. Laugel, and M. Tirrell, "Thermodynamic characterization of polypeptide complex coacervation," Langmuir **28**, 15947–15957 (2012).
[11] C. E. Sing and S. L. Perry, "Recent progress in the science of complex coacervation," Soft Matter **16**, 2885–2914 (2020).
[12] S. Srivastava and M. V. Tirrell, "Polyelectrolyte complexation," in *Advances in Chemical Physics*, edited by S. A. Rice and A. R. Dinner (Wiley-Blackwell, Malden, 2016), Vol. 161, pp. 499–544.
[13] M. Muthukumar, "50th anniversary perspective: A perspective on polyelectrolyte solutions," Macromolecules **50**, 9528–9560 (2017).
[14] Y. Anraku, A. Kishimura, M. Oba, Y. Yamasaki, and K. Kataoka, "Spontaneous formation of nanosized unilamellar polyion complex vesicles with tunable size and properties," J. Am. Chem. Soc. **132**, 1631–1636 (2010).
[15] A. Harada and K. Kataoka, "Formation of polyion complex micelles in an aqueous milieu from a pair of oppositely-charged block-copolymers with poly(ethylene glycol) segments," Macromolecules **28**, 5294–5299 (1995).
[16] K. Kataoka, H. Togawa, A. Harada, K. Yasugi, T. Matsumoto, and S. Katayose, "Spontaneous formation of polyion complex micelles with narrow distribution from antisense oligonucleotide and cationic block copolymer in physiological saline," Macromolecules **29**, 8556–8557 (1996).
[17] H. Oana, M. Morinaga, A. Kishimura, K. Kataoka, and M. Washizu, "Direct formation of giant unilamellar vesicles from microparticles of polyion complexes and investigation of their properties using a microfluidic chamber," Soft Matter **9**, 5448–5458 (2013).

[18]S. L. Perry, L. Leon, K. Q. Hoffmann, M. J. Kade, D. Priftis, K. A. Black, D. Wong, R. A. Klein, I. Pierce, F. Charles, K. O. Margossian, J. K. Whitmer, J. Qin, J. J. de Pablo, and M. Tirrell, "Chirality-selected phase behaviour in ionic polypeptide complexes," Nat. Commun. **6**, 6052 (2015).
[19]C. V. Synatschke, T. I. Löbling, M. Förtsch, A. Hanisch, F. H. Schacher, and A. H. E. Müller, "Micellar interpolyelectrolyte complexes with a compartmentalized shell," Macromolecules **46**, 6466–6474 (2013).
[20]H. M. van der Kooij, E. Spruijt, I. K. Voets, R. Fokkink, M. A. Cohen Stuart, and J. van der Gucht, "On the stability and morphology of complex coacervate core micelles: From spherical to wormlike micelles," Langmuir **28**, 14180–14191 (2012).
[21]I. K. Voets, A. de Keizer, P. de Waard, P. M. Frederik, P. H. H. Bomans, H. Schmalz, A. Walther, S. M. King, F. A. M. Leermakers, and M. A. Cohen Stuart, "Double-faced micelles from water-soluble polymers," Angew. Chem., Int. Ed. **45**, 6673–6676 (2006).
[22]I. K. Voets, R. Fokkink, T. Hellweg, S. M. King, P. d. Waard, A. d. Keizer, and M. A. Cohen Stuart, "Spontaneous symmetry breaking: Formation of Janus micelles," Soft Matter **5**, 999–1005 (2009).
[23]Y. Yan, N. A. M. Besseling, A. de Keizer, M. Drechsler, R. Fokkink, and M. A. Cohen Stuart, "Wormlike aggregates from a supramolecular coordination polymer and a diblock copolymer," J. Phys. Chem. B **111**, 11662–11669 (2007).
[24]Y. Yan, L. Harnau, N. A. M. Besseling, A. de Keizer, M. Ballauff, S. Rosenfeldt, and M. A. Cohen Stuart, "Spherocylindrical coacervate core micelles formed by a supramolecular coordination polymer and a diblock copolymer," Soft Matter **4**, 2207–2212 (2008).
[25]R. Takahashi, T. Sato, K. Terao, and S.-i. Yusa, "Intermolecular interactions and self-assembly in aqueous solution of a mixture of anioniccneutral and cationiccneutral block copolymers," Macromolecules **48**, 7222–7229 (2015).
[26]C. Chassenieux and C. Tsitsilianis, "Recent trends in pH/thermo-responsive self-assembling hydrogels: From polyions to peptide-based polymeric gelators," Soft Matter **12**, 1344–1359 (2016).
[27]S. Srivastava, M. Andreev, A. E. Levi, D. J. Goldfeld, J. Mao, W. T. Heller, V. M. Prabhu, J. J. de Pablo, and M. V. Tirrell, "Gel phase formation in dilute triblock copolyelectrolyte complexes," Nat. Commun. **8**, 14131 (2017).
[28]M. Guvendiren, H. D. Lu, and J. A. Burdick, "Shear-thinning hydrogels for biomedical applications," Soft Matter **8**, 260–272 (2012).
[29]S. Khetan and J. A. Burdick, "Patterning hydrogels in three dimensions towards controlling cellular interactions," Soft Matter **7**, 830–838 (2011).
[30]J. F. Mano, "Stimuli-responsive polymeric systems for biomedical applications," Adv. Eng. Mater. **10**, 515–527 (2008).
[31]B. D. Olsen, J. A. Kornfield, and D. A. Tirrell, "Yielding behavior in injectable hydrogels from telechelic proteins," Macromolecules **43**, 9094–9099 (2010).
[32]C. P. Brangwynne, "Phase transitions and size scaling of membrane-less organelles," J. Cell Biol. **203**, 875–881 (2013).
[33]A. K. Bajpai, S. K. Shukla, S. Bhanu, and S. Kankane, "Responsive polymers in controlled drug delivery," Prog. Polym. Sci. **33**, 1088–1118 (2008).
[34]P. Gupta, K. Vermani, and S. Garg, "Hydrogels: From controlled release to pH-responsive drug delivery," Drug Discovery Today **7**, 569–579 (2002).
[35]T. R. Hoare and D. S. Kohane, "Hydrogels in drug delivery: Progress and challenges," Polymer **49**, 1993–2007 (2008).
[36]N. A. Peppas, "Hydrogels and drug delivery," Curr. Opin. Colloid Interface Sci. **2**, 531–537 (1997).
[37]M. A. C. Stuart, N. A. M. Besseling, and R. G. Fokkink, "Formation of micelles with complex coacervate cores," Langmuir **14**, 6846–6849 (1998).
[38]A. Harada and K. Kataoka, "Chain length recognition: Core-shell supramolecular assembly from oppositely charged block copolymers," Science **283**, 65–67 (1999).
[39]J. N. Hunt, K. E. Feldman, N. A. Lynd, J. Deek, L. M. Campos, J. M. Spruell, B. M. Hernandez, E. J. Kramer, and C. J. Hawker, "Tunable, high modulus hydrogels driven by ionic coacervation," Adv. Mater. **23**, 2327–2331 (2011).
[40]D. V. Krogstad, S.-H. Choi, N. A. Lynd, D. J. Audus, S. L. Perry, J. D. Gopez, C. J. Hawker, E. J. Kramer, and M. V. Tirrell, "Small angle neutron scattering study of complex coacervate micelles and hydrogels formed from ionic diblock and triblock copolymers," J. Phys. Chem. B **118**, 13011–13018 (2014).
[41]D. V. Krogstad, N. A. Lynd, D. Miyajima, J. Gopez, C. J. Hawker, E. J. Kramer, and M. V. Tirrell, "Structural evolution of polyelectrolyte complex core micelles and ordered-phase bulk materials," Macromolecules **47**, 8026–8032 (2014).
[42]D. J. Audus, J. D. Gopez, D. V. Krogstad, N. A. Lynd, E. J. Kramer, C. J. Hawker, and G. H. Fredrickson, "Phase behavior of electrostatically complexed polyelectrolyte gels using an embedded fluctuation model," Soft Matter **11**, 1214–1225 (2015).
[43]S. Srivastava, A. E. Levi, D. J. Goldfeld, and M. V. Tirrell, "Structure, morphology, and rheology of polyelectrolyte complex hydrogels formed by self-assembly of oppositely charged triblock polyelectrolytes," Macromolecules **53**, 5763–5774 (2020).
[44]C. E. Sing, "Development of the modern theory of polymeric complex coacervation," Adv. Colloid Interface Sci. **239**, 2–16 (2017).
[45]S. Friedowitz, A. Salehi, R. G. Larson, and J. Qin, "Role of electrostatic correlations in polyelectrolyte charge association," J. Chem. Phys. **149**, 163335 (2018).
[46]J. Fu and J. B. Schlenoff, "Driving forces for oppositely charged polyion association in aqueous solutions: Enthalpic, entropic, but not electrostatic," J. Am. Chem. Soc. **138**, 980–990 (2016).
[47]M. Radhakrishna, K. Basu, Y. Liu, R. Shamsi, S. L. Perry, and C. E. Sing, "Molecular connectivity and correlation effects on polymer coacervation," Macromolecules **50**, 3030–3037 (2017).
[48]A. Kudlay, A. V. Ermoshkin, and M. Olvera de la Cruz, "Complexation of oppositely charged polyelectrolytes: Effect of ion pair formation," Macromolecules **37**, 9231–9241 (2004).
[49]J. Lee, Y. O. Popov, and G. H. Fredrickson, "Complex coacervation: A field theoretic simulation study of polyelectrolyte complexation," J. Chem. Phys. **128**, 224908 (2008).
[50]I. Michaeli, J. T. G. Overbeek, and M. J. Voorn, "Phase separation of polyelectrolyte solutions," J. Polym. Sci. **23**, 443–450 (1957).
[51]J. T. G. Overbeek and M. J. Voorn, "Phase separation in polyelectrolyte solutions; theory of complex coacervation," J. Cell. Comp. Physiol. **49**, 7–26 (1957).
[52]S. L. Perry and C. E. Sing, "Prism-based theory of complex coacervation: Excluded volume versus chain correlation," Macromolecules **48**, 5040–5053 (2015).
[53]J. Qin and J. J. de Pablo, "Criticality and connectivity in macromolecular charge complexation," Macromolecules **49**, 8789–8800 (2016).
[54]P. Zhang, N. M. Alsaifi, J. Wu, and Z.-G. Wang, "Polyelectrolyte complex coacervation: Effects of concentration asymmetry," J. Chem. Phys. **149**, 163303 (2018).
[55]S. Adhikari, M. A. Leaf, and M. Muthukumar, "Polyelectrolyte complex coacervation by electrostatic dipolar interactions," J. Chem. Phys. **149**, 163308 (2018).
[56]A. Shakya, M. Girard, J. T. King, and M. Olvera de la Cruz, "Role of chain flexibility in asymmetric polyelectrolyte complexation in salt solutions," Macromolecules **53**, 1258–1269 (2020).
[57]A. M. Rumyantsev and J. J. de Pablo, "Microphase separation in polyelectrolyte blends: Weak segregation theory and relation to nuclear 'pasta,'" Macromolecules **53**, 1281–1292 (2020).
[58]T. K. Lytle, M. Radhakrishna, and C. E. Sing, "High charge density coacervate assembly via hybrid Monte Carlo single chain in mean field theory," Macromolecules **49**, 9693–9705 (2016).
[59]T. K. Lytle and C. E. Sing, "Transfer matrix theory of polymer complex coacervation," Soft Matter **13**, 7001–7012 (2017).
[60]G. M. C. Ong and C. E. Sing, "Mapping the phase behavior of coacervate-driven self-assembly in diblock copolyelectrolytes," Soft Matter **15**, 5116–5127 (2019).
[61]S. P. O. Danielsen, J. McCarty, J.-E. Shea, K. T. Delaney, and G. H. Fredrickson, "Molecular design of self-coacervation phenomena in block polyampholytes," Proc. Natl. Acad. Sci. U. S. A. **116**, 8224–8232 (2019).
[62]C. E. Sing, "Micro- to macro-phase separation transition in sequence-defined coacervates," J. Chem. Phys. **152**, 024902 (2020).
[63]A. M. Rumyantsev, E. B. Zhulina, and O. V. Borisov, "Scaling theory of complex coacervate core micelles," ACS Macro Lett. **7**, 811–816 (2018).
[64]D. V. Krogstad, N. A. Lynd, S.-H. Choi, J. M. Spruell, C. J. Hawker, E. J. Kramer, and M. V. Tirrell, "Effects of polymer and salt concentration on the structure

and properties of triblock copolymer coacervate hydrogels," Macromolecules **46**, 1512–1518 (2013).
[65]A. Salehi and R. G. Larson, "A molecular thermodynamic model of complexation in mixtures of oppositely charged polyelectrolytes with explicit account of charge association/dissociation," Macromolecules **49**, 9706–9719 (2016).
[66]A.-C. Shi and J. Noolandi, "Theory of inhomogeneous weakly charged polyelectrolytes," Macromol. Theory Simul. **8**, 214–229 (1999).
[67]J. Jiang, X. Chen, S. Yang, and E.-Q. Chen, "The size and affinity effect of counterions on self-assembly of charged block copolymers," J. Chem. Phys. **152**, 124901 (2020).
[68]S. Yang, Z. Lei, N. Hu, E.-Q. Chen, and A.-C. Shi, "Regulating block copolymer phases via selective homopolymers," J. Chem. Phys. **142**, 124903 (2015).
[69]K. J. Hou and J. Qin, "Solvation and entropic regimes in ion-containing block copolymers," Macromolecules **51**, 7463–7475 (2018).
[70]M. W. Matsen, "The standard Gaussian model for block copolymer melts," J. Phys.: Condens. Matter **14**, R21–R47 (2002).
[71]J.-M. Kim, T.-Y. Heo, and S.-H. Choi, "Structure and relaxation dynamics for complex coacervate hydrogels formed by aba triblock copolymers," Macromolecules **53**, 9234–9243 (2020).